The Effect of Gas Diffusion Layer Compression on Gas Bypass and Water Slug Motion in Parallel Gas Flow Channels

Donghao H. Ye
Dept. of Chemical and Biological Engineering, Princeton University, Princeton, NJ 08544

State Key Laboratory of Advanced Technology for Materials Synthesis and Processing, Wuhan University of Technology, Wuhan 430070, China

Eric Gauthier, May Jean Cheah, and Jay Benziger
Dept. of Chemical and Biological Engineering, Princeton University, Princeton, NJ 08544

Mu Pan
State Key Laboratory of Advanced Technology for Materials Synthesis and Processing, Wuhan University of Technology, Wuhan 430070, China

DOI 10.1002/aic.14686
Published online November 22, 2014 in Wiley Online Library (wileyonlinelibrary.com)

Water slugs form in the gas flow channels of polymer electrolyte membrane fuel cells (PEMFCs) which hinder reactant transport to the catalyst layer. We report a study correlating video images of slug formation and motion with pressure/flow measurements in parallel gas flow channels. Slugs move when the differential gas pressure exceeds the force to advance the contact lines of the slug with the channel walls. Water slugs can divert the gas flow through the gas diffusion layer (GDL) beneath the ribs to adjacent channels. The flow diversion can cause slugs to stop moving. Slug size and motion has been correlated with in situ GDL permeabilities as functions of GDL compression. Compression reduces the GDL permeability under the ribs much more than the GDL permeability under the channel. A model is presented to describe the spatio-temporal location of slugs in a PEMFC flow field. © 2014 American Institute of Chemical Engineers
AIChE J, 61: 355–367, 2015
Keywords: fuel cells, multiphase flow, porous media, microfluidics

Introduction

Polymer electrolyte membrane fuel cells (PEMFCs) are a promising energy conversion technology because of the high energy density of the hydrogen fuel.[1,2] PEMFC power density may be limited by the efficient delivery of gaseous reactants to all portions of the fuel cell. Water drops and slugs generated at the cathode can flood the gas flow channels hindering the delivery of reactant gases to regions of the fuel cell.[3,4]

Numerous configurations of gas flow channel designs have been proposed to limit flooding.[5–13] Li et al.[14] reviewed water flooding in PEMFCs and identified two common strategies to mitigate flooding. One strategy is based on controlling temperature and pressure to remove the water as a vapor or fine drops.[15,16] This approach introduces parasitic power loss associated with water vaporization. The second strategy is based on modifying the wetting and flow properties of the membrane electrode assembly (MEA) and bipolar plates (BP) to facilitate water removal.[17,18] The pore structure and surface wettability of the gas diffusion layer (GDL) and cathode catalyst layer can be modified to direct water flow.[19–24] But the detailed physics of the coupling of flow through the porous layers of the MEA and the gas flow channel is still not fully understood which hinders the development of an optimal strategy for water removal.

Benziger and coworkers have utilized model experimental systems to examine how liquid water flows through the porous GDL and how drops and slugs form and move in gas flow channels.[25–29] Their results showed that liquid water penetrates the largest pores of the GDL, emerges into the gas flow channel and grows into drops and eventually slugs. Slugs form when the cross-section of the gas flow channel becomes occluded. Slug formation is accompanied by a large increase in differential pressure for the gas flow through the channel. Cheah et al. showed that the wettability of the flow channel walls plays a key role in the size of liquid slugs, but the power required to remove slugs was only weakly dependent on slug size.[30]

Several other investigators have also observed slug flow in gas flow channels with emerging water drops. Ody observed regular periodic slug motion in microchannels with rectangular cross-sections.[31] Trabold et al. appears to have been the first to show that the pressure drop for gas flow is a sensitive indicator of slug formation in the gas flow channels.[32] Bazylak et al. investigated the flow regimes for "mist" flow to

Correspondence concerning this article should be addressed to J. Benziger at benziger@princeton.edu.

slug flow from drops emerging from the GDL into a gas flow channel; they observed a transition from slugs to a mist at moderate gas flow rates.[33] Theodorakakos et al. focused on the force required to detach emerging water droplets at high gas flow rates.[34] These studies all implicitly assumed that mixed gas and liquid flow occurred in the gas flow channel, characterized by a single superficial flow velocity. The work by Cheah et al. indicated that gas and liquid flows are separate and are coupled through the boundary conditions at the gas liquid interface.[35] Cheah et al. showed that in flow channels with four solid walls slugs detach almost immediately on formation and move at the superficial gas velocity at moderate gas phase Reynolds number, $Re_G = (Q_G\rho_G)/(w\mu_G) < 30$, where Q_G is the volumetric gas flow, ρ_G is the gas density, w is the channel width, and μ_G is the gas viscosity. They observed that at $Re_G > 70$ drops detach before slug formation the drops move slower than the gas.

PEMFC gas flow channels have three solid walls, generally made of graphite or stainless steel. The fourth wall is the porous hydrophobic gas diffusion layer (GDL) which interfaces with the catalyst layer and the membrane. Cho et al. examined drop detachment from GDL surfaces at high gas velocity.[36] They limited their analysis to situations where drops only touched the GDL surface and observed distorted spherical drops that moved slower than the superficial gas velocity. Hellstern et al. compared drop and slug formation and motion in channels with and without a GDL at low to moderate gas flow rates, $Re_G < 30$. They observed that slugs grew to be much larger in channels with a GDL than in channels with four solid walls.[37] Hellstern showed that in channels with a GDL the water slugs continue to grow after they occlude the cross-section of the gas flow channel. During slug growth the gas flow is diverted through the GDL bypassing the slug. Slugs grow until the force for gas flow through the GDL equaled to the force required to advance the slug's liquid/solid contact lines at which point the slug detaches and moves.

Gas flow through the GDL depends on the permeability of the GDL. The MEA, consisting of the polymer membrane, catalyst layers, and GDLs, is compressed between the PEMFCs BP which contain the gas flow channels. The compression imposed on the MEA alters GDL permeability. There have been a number of studies of the effect of permeability of GDL materials,[38–42] including tomographic studies,[43–46] thermal conduction measurements,[46–48] and electrical measurements.[49] This article examines the influence of compressing the GDL on the gas bypass and the motion of slugs in flow channels. The measurements are done in a mixed gas/liquid flow system which mimics the cathode of an operating fuel cell. We show how the gas permeabilities of the GDL under the channel and under the rib determine slug size as a function of gas flow rate. We also show slugs divert gas flow between adjacent channels resulting in correlated motion of slugs in adjacent channels.

Experimental

Experimental apparatus

A parallel channel flow system was machined from two acrylic blocks as shown in Figure 1. Both channels had three solid acrylic walls and the fourth wall was Toray carbon paper with 20% polytetrafluoro ethylene (PTFE) loading

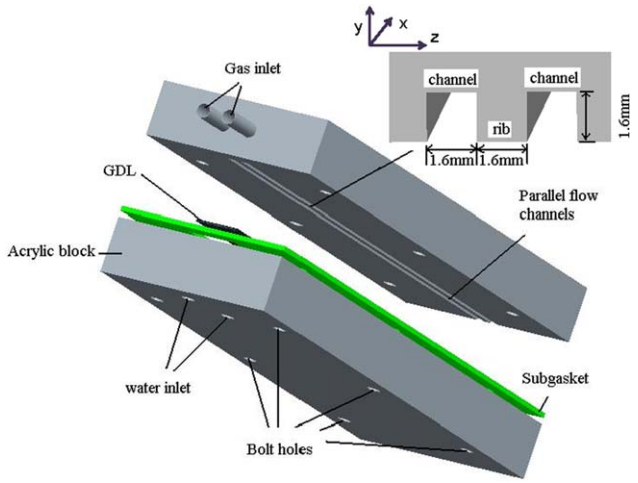

Figure 1. Schematic of the microfluidic flow device.

Gas flow is in the square channels in the *x*-direction. A gas diffusion layer is in the *xz*-plane. [Color figure can be viewed in the online issue, which is available at wileyonlinelibrary.com.]

(TGP-H-120 obtained from the Fuel Cell Store). Two parallel channels 1.6 mm square by 125 mm long separated by a rib 1.6 mm wide were machined into one acrylic block. The channel dimensions are similar to the flow channels in most PEMFCs, which are typically 0.5–1.5 mm wide. The second acrylic block had two 100 μm holes drilled to be centered side to side in the square channels. These holes have similar diameter to the pores in carbon cloth GDL materials and slightly larger than the pores of carbon paper GDL.[27] A strip of Toray paper GDL 5 mm wide by 120 mm long was affixed between the two acrylic blocks with a thin film of silicon grease along the outsides of the channels. A silicon rubber gasket surrounded the GDL material blocking gas flow from exiting laterally. Hundred micrometer holes were punched through the GDL aligned with the holes through the acrylic block. These holes are referred to as the water pores. Water was pumped through these 100 μm pores using two syringe pumps. Nitrogen gas flowed through the square channels; the nitrogen flow rates were controlled by individual mass flow controllers (one for each channel). The differential pressures between the inlets and outlets of both gas flow channels were measured with differential pressure transducers (Omega PX164-005D5V) and logged by computer at 20 Hz. A high speed camera (Phantom V5, Vision Research) recorded video images of the drops and slugs in the channels. The gas flow channels were horizontal with the liquid inlet pore/GDL surface on the bottom of the channel. Water drops emerged from the water pores forming sessile drops that grew into slugs in the gas flow channels.

The carbon paper GDL under the rib was compressed by six bolts clamping the acrylic blocks. The bolts were tensioned uniformly with a torque wrench. The compressive strain ($\Delta t_{GDL}/t_{GDL}$) of the GDL was determined by measuring the spacing between the two acrylic blocks with a micrometer. The pressure on the GDL could not be determined because the clamping force was borne by both the GDL and the silicon gasket. Measurements were carried out at three different compressive strains of the GDL: 4% compression, 12% compression, and 30% compression.

Two types of experiments were carried out. The first set of experiments involved the formation, detachment, and

motion of a single slug in one channel with a large stationary slug partially blocking the second channel. These experiments were carried out to determine the permeability of the carbon paper GDL for different compressions. The second set of experiments involved having continuous water flow into the pores of both channels and continuous gas flow into both channels. Slug size, slug velocity, and differential pressure for slug detachment and motion were measured. These experiments were run generally for 2–3 h, sufficient for a quasiperiodic steady state formation and motion of slugs to be established.

Measuring GDL permeability from slug size and motion

Water emerges from the GDL liquid pore, diameter d_{pore}, into a square gas flow channel with width w; $d_{\text{pore}}/w << 1$ (the experimental system reported here has $d_{\text{pore}}/w = 1/16$). In the studies reported here, the gas flow in the channels was chosen to have gas phase Reynolds numbers $Re_{\text{G}} = Q_{\text{G}}\rho_{\text{G}}/w\mu_{\text{G}} < 36$. This is the range of Re_{G} encountered in PEMFCs with parallel flow channels or in PEMFCs with serpentine flow channels and a fuel cell area $A_{\text{FC}} < 25$ cm^2.[26] The experiments have been carried out with deionized water and N_2 gas. The flow conditions for N_2 gas are similar to those for air flow at the cathode of a PEMFC. The Re numbers for H_2 flow at the anode of a PEMFC are typically an order of magnitude smaller than those tested here.

Colosqui et al.[26] and Hellstern et al.[37] showed that for $Re_{\text{G}} < 30$ sessile water drops in a square channel are pinned to the water inlet pore and grow until they achieve a critical volume where drops are converted to slugs which occlude the channel cross-section. In a channel with four solid walls, Colosqui et al. showed that a periodic "steady state" was obtained where water emerging from the pore grew into slugs that detached and moved down the channel. The differential gas pressure increased from ~1 to ~100 Pa when slugs occluded the flow channel and were moving. The critical drop volume when slugs first form, is w^2L_0, where the length of slugs, L_0, is given by Eq. 1, and θ is the effective static contact angle of water with the channel walls. For $Re_{\text{G}} < 30$, the critical drop volume for slug formation was shown to be independent of the gas flow rate[26,30]

$$L_0 = w\frac{\theta - \frac{1}{2}\sin 2\theta}{(1-\cos\theta)^2} \tag{1}$$

When slugs form in channels with four solid walls, they occlude the cross-section of the gas flow channel. The volumetric gas flow into the channel is fixed, so blocking the gas flow causes the upstream gas pressure to rapidly increase. The slug detaches and moves when the inertial force from the gas pressure pushing on the slug exceeds the force to advance the gas/liquid/solid contact lines at the perimeter of the front and back of the slug. The pressure required to detach the slug is given by Eq. 2

$$\Delta P_{\text{detachement}} = \frac{1}{w^2}\int_{\substack{\text{channel}\\ \text{perimeter}}} \gamma_w(\cos\theta_{\text{R}} - \cos\theta_{\text{A}})\hat{n}\cdot dl \tag{2}$$

where γ_{w} is the surface tension of water and θ_{A} and θ_{R} are the advancing and receding contact angles of water with the channel walls.

When one wall of the gas flow channel is comprised of a porous GDL slugs do not detach when first formed. Hellstern et al. showed that gas flows through the GDL, bypassing the slug, allowing the slug to continue growing.[37] When the slug length, L_{slug}, is sufficiently long the differential pressure for the gas flow through the GDL exceeds the differential pressure required to advance the gas/liquid/solid contact lines and the slug detaches and begins to move.

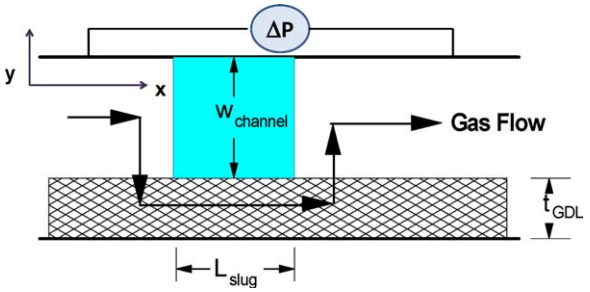

Figure 2. Schematic of the gas flow bypassing the slug and flow through the porous gas diffusion layer in the *xy* direction.

The large arrows trace the path of gas flow bypassing the water slug in the channel. [Color figure can be viewed in the online issue, which is available at wileyonlinelibrary.com.]

Figure 2 illustrates the gas flow bypassing a water slug in the gas flow channel. Figure 2 is an xy projection of a single flow channel. The x-direction is along the direction of gas flow and the y-direction is from the GDL at the bottom of the channel to the solid wall at the top of the channel. The differential pressure across the drop in the direction of gas flow is measured as indicated in Figure 2. The differential pressure for the gas to flow through the GDL beneath the slug depends on the slug length, gas flow rate, and the permeability of the GDL under the channel, $k_{\substack{\text{GDL}\\ \text{channel}}}$; it may be approximated by Darcy's law, given by Eq. 3

$$\Delta P_{\substack{\text{gas}\\ \text{flow}}} = \frac{L_{\text{slug}}Q_{\text{G}}\mu_{\text{G}}}{k_{\substack{\text{GDL}\\ \text{channel}}} wt_{\substack{\text{GDL}\\ \text{channel}}}} \tag{3}$$

where t_{GDL} is the thickness of the GDL.

When the slug achieves the critical length to detach and move, all the gas flow is being forced through the GDL, beneath the slug. The pressure drop associated with the gas flow through the GDL equals the pressure drop required for slug detachment, $\Delta P_{\substack{\text{gas}\\ \text{flow}}} = \Delta P_{\text{detachment}}$. The differential pressure for slug detachment in a channel with three acrylic walls and a GDL wall is given by integrating Eq. 2 along the contact perimeters, yielding Eq. 4

$$\Delta P_{\text{detachment}} = \frac{\gamma_w}{w}\left(3(\cos\theta_{\text{R}} - \cos\theta_{\text{A}})_{\text{acrylic}} + (\cos\theta_{\text{R}} - \cos\theta_{\text{A}})_{\text{GDL}}\right) \tag{4}$$

The detachment pressure for slugs is independent of the slug volume; it only depends on the contact perimeter at the two gas/liquid/solid interfaces. In a typical experiment, the channel geometry is fixed and the detachment pressure and the slug length are measured as functions of Q_{G}. All the parameters in Eq. 3 are known except for the GDL permeability. This permits the evaluation of the permeability of the GDL under the channel.

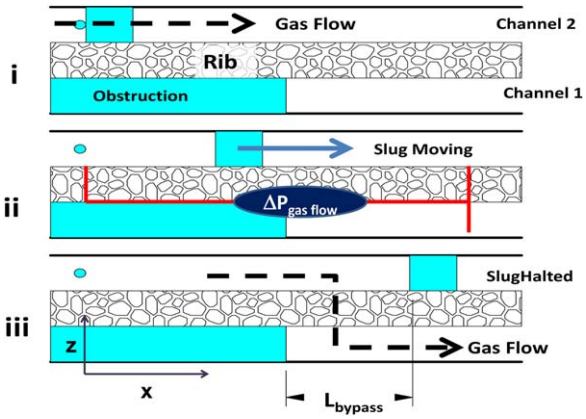

Figure 3. Slug motion in parallel channels with an obstruction in one channel viewed from the *xz*-plane.

Water enters Channel 2 through a 100 μm pore near the channel entrance. (i) Drop grows to a slug in Channel 1; (ii) Slugs grow and detach when the differential pressure for gas flow through the GDL beneath the slug exceeds the pressure required for slug motion; (iii) Slugs stop moving and the gas flow is diverted through the GDL under the rib from Channel 2 into Channel 1. [Color figure can be viewed in the online issue, which is available at wileyonlinelibrary.com.]

When two parallel channels share a common GDL, gas can flow through the GDL under the rib from one channel into the adjacent channel. Figure 3 illustrates two parallel gas flow channels which share a common GDL as found in PEM fuel cells. Figure 3 is in the view from the *xz*-plane, looking from above the two channels. The two channels are separated by a rib which compresses the GDL beneath it. The bottom surface of both channels is uncompressed GDL. Channel 1 has no gas feed and is partially filled with a stationary water slug (labelled the obstruction). Gas flows in Channel 2 entering from the left in Figure 3. Water is fed to Channel 2 through a single pore through the GDL near the gas inlet to Channel 2. The differential gas pressure is measured between the gas inlet to Channel 2 and the outlet to Channel 2, ΔP_{22}. The outlets to Channels 1 and 2 are both open to the atmosphere so the differential pressure between the inlet to Channel 2 and the outlet to Channel 1, ΔP_{21}, is equal to ΔP_{22}.

Water emerges from the pore in Channel 2 and grows to be a slug. ΔP_{22} is small until the slug forms in Channel 2 (Figure 3i). Once a slug forms in Channel 2, ΔP_{22} increases. The slug grows and ΔP_{22} increases until the differential pressure across the slug in Channel 2 exceeds the slug detachment pressure, at which point the slug detaches and starts to move (Figure 3ii). To simplify the analysis of slug motion, the water flow to the pore in Channel 2 was stopped when the slug detached and started moving; this avoided ambiguities associated with a second slug in the gas flow channel. When the slug in Channel 2 is moving and is adjacent to the obstruction slug in Channel 1 ΔP_{22} is approximately constant.

Once the slug in Channel 2 moves past the obstruction slug in Channel 1, it slows down and eventually comes to a stop at a distance L_{bypass} downstream from the obstruction slug (Figure 3iii). When the slug is slowing down ΔP_{22} decreases and becomes constant when the slug stops. Between the end of the water obstruction in Channel 1 and the stalled slug in Channel 2 a fraction of the gas that enters Channel 2 flows beneath the rib from Channel 2 into 1 and exits from Channel 1, as illustrated in Figure 3iii. The remaining gas flows beneath the stalled slug in Channel 2 and exits from Channel 2. The differential pressure, ΔP_{22}, for those two flow paths must be the same and must also equal to the detachment pressure to advance the contact lines for the slugs.

The gas flow from Channel 2 beneath the rib to Channel 1, $Q_{\underset{2\to1}{\text{G}}}$, may be approximated by Darcy's Law as shown in Eq. 5

$$Q_{\underset{2\to1}{\text{G}}} = \frac{\Delta P_{\underset{\text{bypass}}{\text{gas}}}\, k_{\underset{\text{rib}}{\text{GDL}}}\, L_{\text{bypass}}\, t_{\underset{\text{rib}}{\text{GDL}}}}{w\mu_{\text{G}}} \tag{5}$$

where $k_{\underset{\text{rib}}{\text{GDL}}}$ is the permeability of the GDL under the rib, L_{bypass} is the bypass distance, $t_{\underset{\text{rib}}{\text{GDL}}}$ is the thickness of the gas diffusion layer under the rib, and $\Delta P_{\underset{\text{bypass}}{\text{gas}}} = \Delta P_{22}$ is the pressure differential between Channel 2 upstream of the slug and Channels 1 and 2 downstream of the slug.

The total gas flow fed to Channel 2, Q_{G}, is partitioned between the gas that flows from Channel 2 to 1 and the gas that passes beneath the stalled slug in Channel 2 ($Q_{\underset{\text{bypass}}{\text{slug}}}$)

$$Q_{\text{G}} = Q_{\underset{2\to1}{\text{GDL}}} + Q_{\underset{\text{bypass}}{\text{slug}}} \,. \tag{6}$$

The slug in Channel 2 stalls when the differential pressure across the slug in Channel 2 is equal to the detachment pressure which is also equal to the differential pressure for gas flow underneath the rib, that is, $\Delta P_{\underset{\text{flow}}{\text{gas}}} = \Delta P_{\underset{\text{bypass}}{\text{gas}}} = \Delta P_{\text{detachment}}$. We have neglected the gas flow that passes beneath part of the stalled slug and then passes beneath the rib into Channel 1.

Equations 3 and 5 were combined with Eq. 6 to yield Eq. 7 which expresses the bypass distance as a function of the gas flow rate

$$L_{\text{bypass}} = \left(\frac{w\mu_{\text{G}}}{\Delta P_{\text{detachment}}\, k_{\underset{\text{rib}}{\text{GDL}}}\, t_{\underset{\text{rib}}{\text{GDL}}}} \right) Q_{\text{G}} - \frac{w^2 k_{\underset{\text{channel}}{\text{GDL}}}\, t_{\underset{\text{channel}}{\text{GDL}}}}{L_{\text{slug}}\, k_{\underset{\text{rib}}{\text{GDL}}}\, t_{\underset{\text{rib}}{\text{GDL}}}} \tag{7}$$

The GDL permeability under the rib can be found from the slope of L_{bypass} vs. Q_{G}, and the GDL permeability under the channel can be found from the intercept.

Results

Measuring GDL permeability

A series of measurements of differential pressure, slug length, and slug bypass distance as functions of the inlet gas flow rate were made at different levels of GDL compression. Figures 4 and 5 show data obtained for GDL compression of ~4% and liquid flow rate to Channel 2 of 10 μL-water min^{-1}. The gas flow rate to Channel 2 was varied from 12 to 100 mL min^{-1} ($4 < Re_{\text{G}} < 36$). Figure 4 shows the differential pressure between the gas inlet and gas outlet of

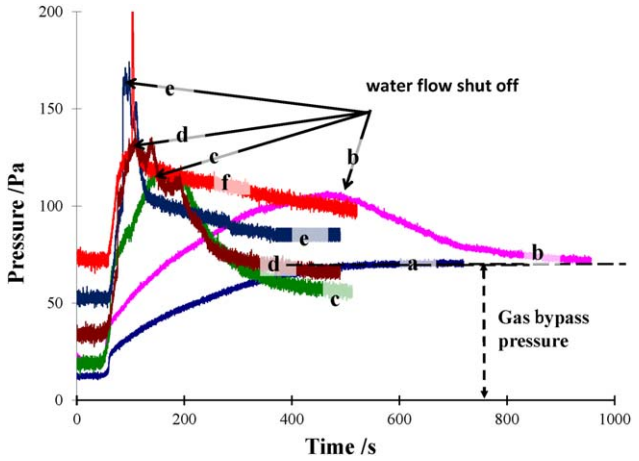

Figure 4. Pressure vs. time for drop growth, slug formation, growth, detachment, and motion in parallel channels with one channel partially obstructed.

The parallel channel arrangement is shown in Figure 3. Channel 1 was partially filled with water. Gas and liquid were fed to Channel 2. The liquid flow rate was 10 μL min^{-1}. Water flow was stopped when the slugs detached as shown. The gas flow rates were (a) 12 mL min^{-1}, (b) 20 mL min^{-1}, (c) 26 mL min^{-1}, (d) 50 mL min^{-1}, (e) 75 mL min^{-1}, (f) 100 mL min^{-1}. [Color figure can be viewed in the online issue, which is available at wileyonlinelibrary.com.]

Channel 2, ΔP_{22}, vs. time. Figure 5 is a set of photographs of the *xz*-plane that shows the final slug length, L_{slug}, and slug position, from which L_{bypass} is determined.

The water obstruction in Channel 1, as shown in Figure 5, does not change with inlet gas flow rate to Channel 2. Water slugs form, detach, move, and finally stall in Channel 2. Figure 5 shows the final location of the slugs in Channel 2 after motion has stalled. Figures 5a–f correspond to increasing gas feed rate to Channel 2. The slugs in Channel 2 and the water obstruction in Channel 1 have been colored with Photoshop^{TM} for clarity. The photographs show the first 60 mm of the total channel length of 125 mm.

The sequence of slug formation, detachment and stalling can be identified from the differential pressure versus time traces shown in Figure 4. The obstruction slug was formed by partial filling Channel 1 with water. There was no inlet gas flow to Channel 1. Steady gas flow was established in Channel 2. There was a constant differential pressure for gas flow in Channel 2 that increased with increasing volumetric flow rate. Water flow through the pore in Channel 2 was started at $t = 0$. For the first ~50 s ΔP_{22} remained constant. During this period, growing drops partially blocked the gas flow channel posing little resistance to the gas flow. ΔP_{22} jumped at ~50 s corresponding to the formation of slugs which spanned the open area of the gas flow channel. The time for slug formation only depends on the liquid flow rate and is independent of gas flow for gas phase Reynolds' number $Re_G < 30$.[30] After slug formation, the differential pressures increases with time; the greater the gas flow rate the faster the differential pressure increased. Slugs detached and moved once the differential pressure increased by ~90 Pa above background pressure for gas flow with no liquid flow. After detachment, the slug moved down Channel 2 at constant velocity until it moved past the obstruction in Channel 1, at which point the slug velocity and the differential pressure both decreased. The slug eventually stopped moving and the differential pressure leveled to a final plateau value of ~80–110 Pa.

Figure 5 shows the final slug positions for different gas flow rates. At the lowest gas flow rate of 12 mL min^{-1} ($Re_G = 4.3$), the slug formed in Channel 2 grew to ~55 mm, exceeding the length of the obstruction in Channel 1. The experiment was terminated after 700 s without slug detachment. The differential pressure shown in Figure 4 increased gradually as the slug grew approaching a final value of ~90 Pa. When $Re_G = 4$ the differential pressure never showed a maximum. The differential pressure for gas flow bypassing the slug never exceeded the detachment pressure.

Increasing the gas flow rate to 20 mL min^{-1} ($Re_G = 7.2$) resulted in slug detachment. It can be seen in Figure 5 that the slug grew to a length of ~40 mm and then detached and moved about 25 mm; but the slug did not move fully past the obstruction slug in Channel 1. Figure 4 shows that the differential pressure went through a maximum of ~100 Pa at 450 s; the maximum in differential gas pressure corresponds to the time when the slug in Channel 2 detached. After the gas detached, the differential gas pressure declined. The slug in Channel 2 stopped moving at ~800 s and the differential gas pressure leveled off at ~90 Pa. When the slug in Channel 2 stopped moving the gas flow was diverted from under the slug in Channel 2 to the open area of Channel 1, which reduced the differential pressure across the length of the slug and resulted in the slug stalling. The final differential pressure approached the same limiting plateau value of ~90 Pa.

When the gas flow rate was increased to 26 mL min^{-1} ($Re_G = 9.4$), the slug grew to ~10 mm and detached. Slug detachment occurred when the differential gas pressure went through a maximum of ~110 Pa. After the slug moved past the stationary slug in Channel 1, the differential gas pressure in Channel 2 decreased and the slug slowed down. The

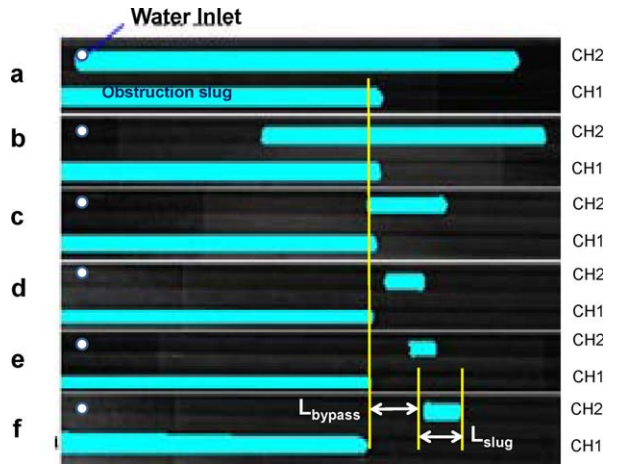

Figure 5. Photographs viewed from the *xz*-plane showing the final size and position of slugs formed in Channel 2 (top channel) with an obstruction slug in Channel 1 (low channel).

The liquid flow rate was 10 μL min^{-1}. Water flow was stopped when the slugs detached as shown. The gas flow rates were (a) 12 mL min^{-1}, (b) 20 mL min^{-1}, (c) 26 mL min^{-1}, (d) 50 mL min^{-1}, (e) 75 mL min^{-1}, (f) 100 mL min^{-1}. [Color figure can be viewed in the online issue, which is available at wileyonlinelibrary.com.]

Table 1. Gas Flow, Slug Length and Detachment Pressure for Carbon Paper GDL

GDL Compression	Minimum Gas Flow for Slug Motion (mL min^{-1})	Slug Length at Detachment (cm)	Differential Pressure for Slug Motion (Pa)	$k_{\underset{\text{channel}}{\text{GDL}}}$ (m^2)
4%	$Q_G \sim 20$	~11.0	90	6.5×10^{-10}
12%	$Q_G \sim 12$	~8.0	90	4.8×10^{-10}
30%	$Q_G \sim 6$	~6.5	90	3.0×10^{-10}

differential pressure decreased to a final value of 90 Pa at which point the slug stopped moving.

Increasing the gas flow rate further decreased the slug length and increased the bypass distance. These results can be explained by force balances. Detachment occurs when force for slug motion equals the force for gas flow beneath the slug. The force to detach and move the slug is independent of slug size and gas flow rate. The force for flow through the GDL scales linearly with slug length and inversely with gas flow rate; slug size at detachment scales inversely with gas flow rate.

Slug detachment occurs when the differential pressure goes through a maximum. The differential gas pressure then decreases a final stead value of ~90 Pa when the slug stops moving. The differential pressure when slugs stall is independent of gas flow rate.

The permeability of the GDL under the channel may be determined from the minimum gas flow for slug detachment using Eq. 3. It is evident from Figures 4 and 5 that the minimum gas flow rate for slug detachment is when $Q_G = 20$ mL min^{-1}, differential pressure for gas flow, $\Delta P_{\underset{\text{flow}}{\text{gas}}} = 90$ Pa (from Figure 4), $L_{slug} = 11.0$ cm (from Figure 5), $w = 0.16$ cm, $t_{GDL} = 0.028$ cm, and $\mu_G = 18$ μPa s. Similar measurements were repeated for a carbon paper GDL compressed to 12% and 30%. Table 1 summarizes the results for slug detachment: gas flow rate, differential pressure, and slug length. Those data were used with Eq. 3 to determine the GDL permeability under the channel.

The permeability under the channel decreases with increased compression. Even though the GDL is not directly compressed under the channel, the compression of the GDL under the ribs causes some compression at the edges of the channel. In addition, a small fraction of the gas flow that bypasses the slugs in the channel also passes under the ribs and that flow is reduced by compression.

The permeability of the GDL under the ribs can be evaluated from the slope of the bypass distance, as a function of the gas flow rate, using Eq. 8. Figure 6 plots the distance a slug in Channel 2 bypasses the obstruction in Channel 1 (L_{bypass}) as a function of the gas flow rate (Q_G). Table 2 summarizes the permeability under the rib as a function of compression

$$k_{\underset{\text{rib}}{\text{GDL}}} = \frac{w\mu_G}{\Delta P_{\text{detachment}} t_{\underset{\text{rib}}{\text{GDL}}} (\text{slope})} \tag{8}$$

At the lowest compression, the permeability of the GDL under the rib and under the channel are almost the same, as expected. However, as the compression is increased the permeability under the rib decreased by more than an order of magnitude (Table 2), while the permeability under the rib decreased by a factor of 2.

Experimental measurements were repeated 2–3 times with the same GDL. The compression experiments were done twice starting with a fresh GDL and sequentially increasing the compression to 4%, 12%, and 30%. The pressure for slug detachment is reproducible to +/−10%. Slug volumes were reproducible to +/−15%. The bypass distances had the largest error of +/−30%.

Slug motion in adjacent channels

The formation, detachment, and motion of slugs in adjacent channels were examined using same parallel channel system as used to measure the GDL permeability. But now, water and gas were supplied at steady rates to both channels. The water pores were staggered between the two channels as shown in Figure 8B; the water pore in Channel 1 was 12 mm from the gas inlet and the water pore in Channel 2 was 25 mm from the gas inlet. The gas and liquid flow rates to both channels were independently controlled. The gas flows in Channels 1 and 2 were cocurrent. The differential gas pressures between the gas inlets and outlets of both channels were measured as a function of time. Videos were taken of the two channels from above (the *xz*-plane) and the motion of water slugs was correlated with the differential pressure traces.

Figure 7 is an example of the differential pressure measurements for the two channels as functions of time. The liquid and gas feed rates were the same for both channels. A horizontal line at 150 Pa shows the detachment pressure for a slug in a single channel. Time zero is defined as when the water flow was initiated to the two channels. For the first 50 s, the differential pressures in both channels are ~10 Pa corresponding to the differential pressure for gas flow through channel with not slugs. After 50 s slugs formed and detached in both channels. During the time period of 50–300 s, the differential pressure traces are complex. The pressures frequently exceeded the detachment pressure for a

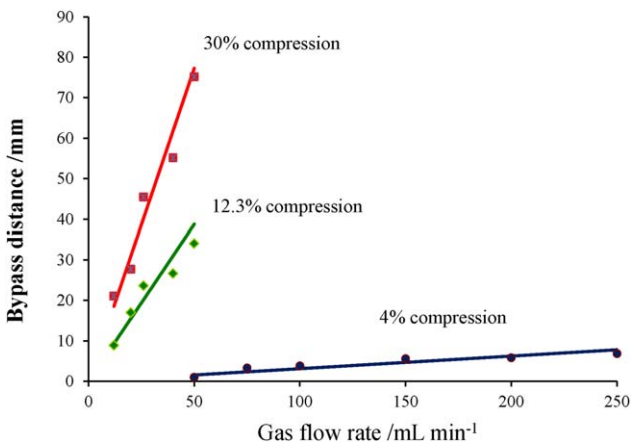

Figure 6. Bypass distance as a function of gas flow rate for slug moving past a stationary obstruction in an adjacent channel.

[Color figure can be viewed in the online issue, which is available at wileyonlinelibrary.com.]

Table 2. Permeability of GDL Under the Rib Between Channels at Different GDL Compressions

GDL Compression	$k_{\substack{\text{GDL}\\\text{rib}}}$ (m^2)
4%	5.0×10^{-10}
12%	3.7×10^{-11}
30%	1.3×10^{-11}

slug. The video images showed that there were multiple slugs in the channels at those times. At times >300 s the pressure traces reached a quasiperiodic steady state where detachment and motion of the slugs in the two channels appeared to be correlated.

At "steady state" the pressure trace in Channel 1 resembled the pressure traces for slug formation is a single isolated channel.[26,30,37] The differential pressure in Channel 1 was ~10 Pa while drops grow at the inlet water pore. When drops grow large enough and become slugs, the differential pressure increases rapidly. The slugs grow and the differential pressure continues to increase gradually. The slugs grow until the differential pressure is equal to the slug detachment pressure. The slug detaches from the inlet water pore and moves down the channel with nearly constant differential pressure of 150 Pa. When slugs exit the channel the differential pressure drops to near zero and the process repeats.

In the quasiperiodic "steady state" for $t > 300$ s, the pressure trace in Channel 2 is not as regular as in Channel 1. When the differential pressure in Channel 1 is ~10 Pa, the differential pressure in Channel 2 varies between 50–90 Pa. Within a few seconds after the slug in Channel 1 detaches the differential pressure in Channel 2 rapidly increases and the slug in Channel 2 detaches. And when slugs exit Channel 1 causing the differential pressure to decrease to near zero, the differential pressure also decreases in Channel 2 but to a differential pressure of ~50–90 Pa.

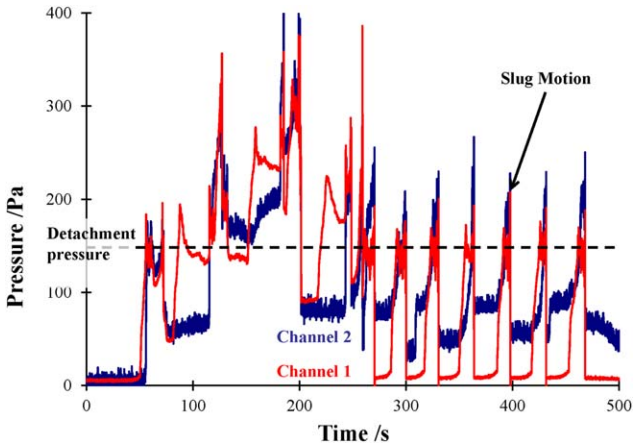

Figure 7. Sample differential pressure traces from two gas flow channels separated by a carbon paper GDL compressed by 12%.

The liquid feed to both channels was 10 μL min^{-1}. The gas feed to both channels was 12 mL min^{-1}. The liquid flow to both channels was initiated at $t = 0$. The differential pressure in Channel 1 is in red and the differential pressure in Channel 2 is in blue. The horizontal line at 150 Pa is the pressure for slug detachment in a single isolated flow channel. [Color figure can be viewed in the online issue, which is available at wileyonlinelibrary.com.]

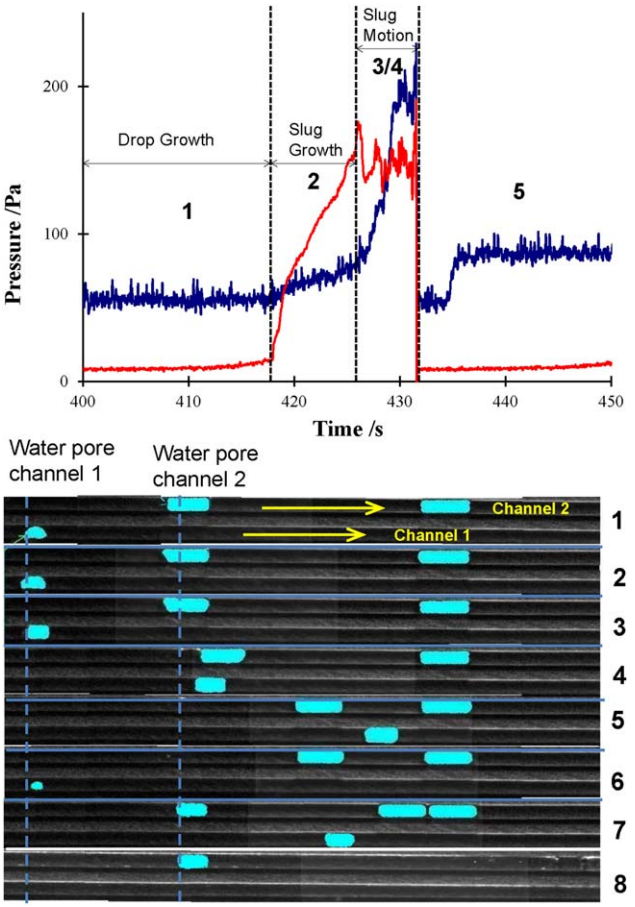

Figure 8. Correlation of Video Images with differential pressure traces for gas/liquid flow in parallel channels.

(A) The differential pressure traces show a sequence of events that are correlated with snapshots of drop motion in the two channels. (B) The video images from the *xz*-plane show ~50 mm of the 125 mm long channels. The inlet water pores are 12 and 25 mm from the gas inlets of Channels 1 and 2, respectively. The water drops/slugs have been highlighted with Photoshop™ to assist the reader. The images were obtained after "quasi" steady state was achieved. A detailed summary of the events at times 1–8 is provided in Table 3. [Color figure can be viewed in the online issue, which is available at wileyonlinelibrary.com.]

Figure 8 is an expanded view of the differential pressure traces for one period of slug formation and motion along with a series of photographs from the *xz*-plane during that same time period. Drops and slugs have been colored to make them easier to identify. The drop growth, slug formation, and slug motion in Channel 1 appears to be independent of Channel 2; slugs form, detach, move, and exit the channel. But the slug detachment and motion in Channel 2 is dependent on the slug motion in Channel 1. Slugs in Channel 2 are distinctly larger than those in Channel 1. Slugs in Channel 2 only move when the slugs in Channel 1 are adjacent to them. Slugs in Channel 2 stall and stop moving after slugs in Channel 1 move past. The correlation of slugs' motion between adjacent channels is a consequence of gas flow between channels through the GDL underneath the rib.

Table 3 summarizes the state of gas flow with drop growth, slug formation, and slug motion at the different time

Table 3. Correlated Motion of Slugs in Adjacent Flow Channels

Time Period	Gas Flow Channel 1 Gas Flow	Gas Flow Channel 2 Gas Flow	Drop/Slug Motion Channel 1 Liquid Flow	Drop/Slug Motion Channel 2 Liquid Flow
1	Flow through open area of Channel 1	Flow split between flow beneath slugs in Channel 2 and flow diverted to Channel 1	Drop growth	Upstream drop/slug growth Downstream slug stationary
2/3	Flow passes beneath slug in Channel 1 and then flows downstream in Channel 1	Flow split between flow beneath slugs in Channel 2 and flow diverted to Channel 1	Slug growth/slug detachment	Upstream slug growth Downstream slug stationary
4	Flow split between flow beneath slug in Channel 1 and pushing slug in Channel 1	Flow beneath slug in Channel 2	Slug motion in Channel 1	Upstream Slug detaches Downstream slug stationary
5	Flow split between flow beneath slug in Channel 1 and pushing slug in Channel 1	Flow beneath slug in Channel 2	Slug moves downstream in Channel 1 with near constant velocity	Upstream slug moves and slows down Downstream slug stationary
6	Flow through open area of Channel 1	Flow split between flow beneath slugs in Channel 2 and flow diverted to Channel 1	Slug exits Channel 1, new drop growing at Channel 1 pore	Upstream slug stalls Downstream slug remains stationary New drop growing at Channel 2 pore

segments annotated on Figure 8. Slugs grow to be larger in Channel 2 because the gas flow is diverted from Channel 2 to 1. The flow diversion reduces the differential pressure for gas flow beneath the slug in Channel 2 so slugs grow longer. When slugs in Channel 1approach slugs in Channel 2 (time 4 in Figure 8) the gas flow can no longer be diverted from Channel 2 into 1, which causes the differential pressure to rise in Channel 2 and the slug starts to move. Because of the second stalled slug in Channel 2, the differential pressure across the moving slug in Channel 2 is less than the differential pressure across the slug in Channel 1. The slug in Channel 2 slows down and stalls while the slug in Channel 1 continues to move and exits the channel.

The effects of compression, gas flow rates, and liquid flow rates on the dynamics of the correlated motion of slugs in adjacent channels were examined. The results summarized below are taken for "steady state" slug formation and motion, that is, after quasiperiodic flows are observed. Figures 9 and 10 compare the pressure traces for two different compression levels. Slug motion is correlated at both compression levels. However, there is a much tighter correlation between the adjacent channels at the higher compression level. The frequency of slug formation is also greater at the higher compression level, because there is less gas flow diversion between adjacent channels through the GDL.

Reducing liquid feeds to Channels 1 and 2 at the same gas flow and GDL compression reduces the frequency of slug formation, which can be seen by comparing Figures 10 and 11. The baseline pressure in Channel 2 is independent of liquid flow rate indicating that the pressure drop associated with gas diversion from Channel 2 into Channel 1 is unchanged with increased liquid flow.

Figures 10 and 12 are pressure traces with the same liquid flow and GDL compressions, only the gas flow was changed. Increased gas flow did not alter the frequency of slug formation, but it did decrease the transit time for slug motion in the gas flow channel. Transit time is the width of the differential pressure peak; peak widths for slug motion are reduced in Figure 12 compared to Figure 10. The baseline pressure for gas flow in Channel 2 is greater at higher gas flow.

Figures 13 and 10 compare pressure traces for the same liquid flows to both channels and the same GDL compression but different gas flow to the two channels. The ratio

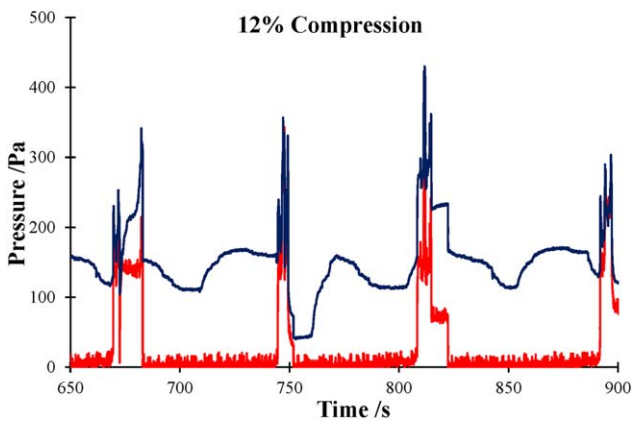

Figure 9. Steady state pressure traces for gas/liquid flows in parallel flow channels with 12% compression of the GDL layer.

The $Q_{G1} = Q_{G2} = 12$ mL min^{-1}; $Q_{L1} = Q_{L2} = 10$ μL min^{-1}. The pressure for Channel 1 is in red and Channel 2 is in blue. [Color figure can be viewed in the online issue, which is available at wileyonlinelibrary.com.]

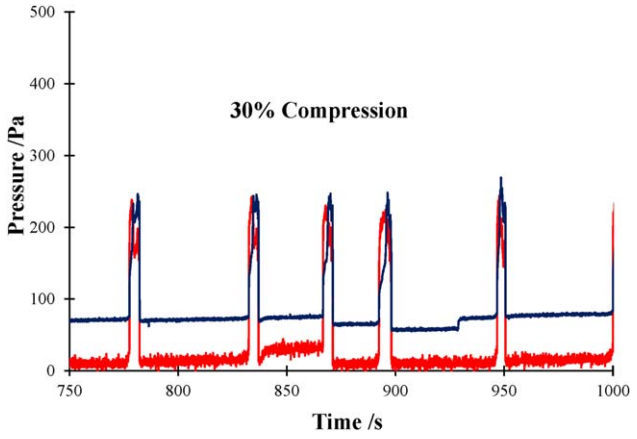

Figure 10. Steady state pressure traces for gas/liquid flows in parallel flow channels with 30% compression of the GDL layer.

The $Q_{G1} = Q_{G2} = 12$ mL min^{-1}; $Q_{L1} = Q_{L2} = 10$ μL min^{-1}. The pressure for Channel 1 is in red and Channel 2 is in blue. [Color figure can be viewed in the online issue, which is available at wileyonlinelibrary.com.]

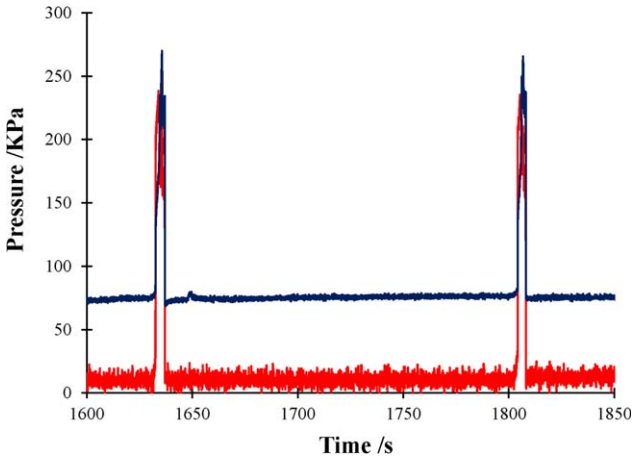

Figure 11. Differential pressure trace for gas/liquid flow in parallel flow channels.

30% GDL compression; $Q_{G1} = Q_{G2} = 12$ mL min^{-1}; $Q_{L2} = 3$ μL min^{-1}. This result should be compared with Figure 10, which is the same compression and gas flow rate, but at a greater liquid flow rate. [Color figure can be viewed in the online issue, which is available at wileyonlinelibrary.com.]

Q_{G1}/Q_{G2} was 2 in Figure 13 and 1 in Figure 10. With different gas flow rates there are multiple frequencies of slug formation and motion. With $Q_{G1}/Q_{G2} = 2$, Channel 2 always has a slug that has stalled. But in Channel 1, half the time there are downstream slugs in the channel and half the time the Channel is clear.

Discussion

The key result from this study is that gas and liquid flows are spatially and temporally coupled for slug motion in gas flow channels. Water slugs can divert the gas to flow beneath the ribs to adjacent channels. Water slug motion is dependent on the locations of other slugs in the same or adjacent gas flow channels. In a PEM fuel cell, the presence of water slugs in the cathode's gas flow channels will result in spatial

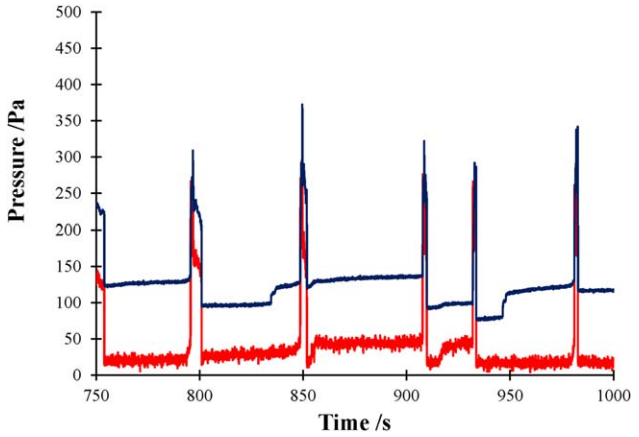

Figure 12. Differential pressure trace for gas/liquid flow in parallel flow channels.

30% GDL compression; $Q_{G1} = Q_{G2} = 20$ mL min^{-1}. $Q_{L1} = Q_{L2} = 10$ μL min^{-1}. This result should be compared with Figure 10, which is the same compression and liquid flow rate, but at a lower gas flow rate. [Color figure can be viewed in the online issue, which is available at wileyonlinelibrary.com.]

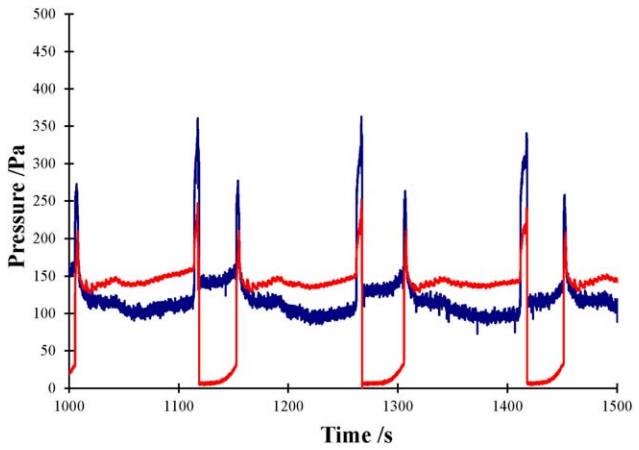

Figure 13. Differential pressure trace for gas/liquid flow in parallel flow channels.

30% GDL compression; $Q_{G1} = 20$ mL min^{-1} and $Q_{G2} = 10$ mL min^{-1}; $Q_{L1} = Q_{L2} = 10$ μL min^{-1} in both channels. This result should be compared with Figure 10, which is the same compression and liquid flow rate, but with the same gas flow rate in both channels. [Color figure can be viewed in the online issue, which is available at wileyonlinelibrary.com.]

and temporal variations of the gas flow rates, gas compositions, and current densities.

The parasitic power for air to flow through the cathode flow channels is equal to the gas flow rate multiplied by the differential pressure between the inlet and outlet. The differential pressure depends on the number and locations of water slugs in the cathode flow channels. Water slugs also divert the gas flow causing some areas of the fuel cell to be starved for reactant resulting in reduced local current density. Kimball et al. showed that in a single flow channel fuel cell the formation and motion of slugs led to spatial and temporal oscillations of the current density along the length of the flow channel.[28] Here, our objective is to characterize slug formation and motion and identify the differential pressure for gas flow in a simplified two channel geometry. Subsequent papers will examine drop and slug flows at higher Re_G and will also examine the role of corners such as those found in serpentine flow fields.

GDL permeability

The size of slugs and the force to move them depends on the permeability of the GDL for gas flow. Permeability can be determined from gas flow measurements through a sheet of GDL material. But those measurements typically do not include the effects of nonuniform compression of the GDL by BP or the effects of liquid slugs in the channels. The GDL permeability measurements reported here attempts to mimic the *in situ* fuel cell environment.

The results summarized in Tables 1 and 2 show that the permeability of the GDL under the channel is greater than the permeability under the rib, and the difference is greater with greater compression. The permeability values are of the same magnitude of values reported in the literature.[39,40,50] There are also few measurements of in-plane permeability of GDL materials under compression for gases which are in semiquantitative agreement with the values reported in Tables 1 and 2.[42,51]

Synchronized flow in adjacent channels

The correlated slug motion in adjacent flow channels occurs because gas flow through the GDL under the ribs

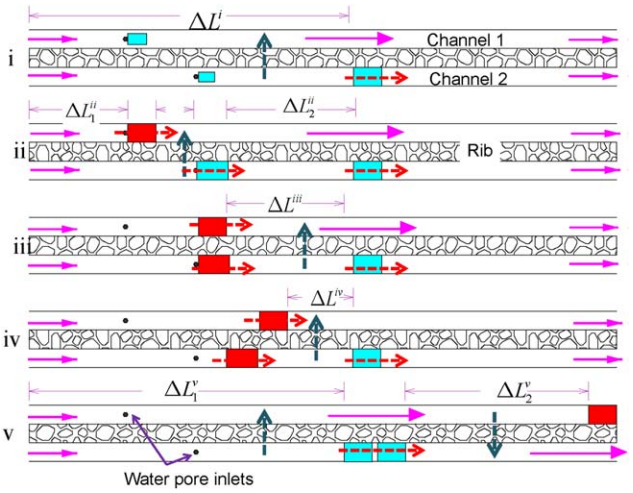

Figure 14. Schematic of slug motion in parallel channels viewed in the *xz*-plane.

Red designates a moving slug, blue are stationary drops or slugs. The horizontal dashed lines (red) designate flow through the GDL underneath a slug. The vertical dashed lines (blue) designate flow through the GDL underneath a rib. (i) Drops growing in Channels 1 and 2 at the water pores, there is a stationary slug stalled downstream in Channel 2. (ii) Slugs form in Channels 1 and 2, the slug in Channel 1 detaches, the slug in Channel 2 remains stationary because of a smaller differential pressure across the slug. (iii) Slug in Channel 1 is adjacent in to slug in Channel 2, which causes the slug in Channel 2 to detach and begin to move. (iv) Slug in Channel 1 moves faster than the slug in Channel 2 because the downstream slug in Channel 2 reduces the differential pressure in across the moving slug in Channel 2. (v) Slug in Channel 2 stalls next to the stationary slug in Channel 2, slug in Channel 1 proceeds downstream and exits the channel. [Color figure can be viewed in the online issue, which is available at wileyonlinelibrary.com.]

becomes unfavorable when slugs are next to each other in adjacent channels. Only a few studies have considered the coupling of gas flow through the GDL and in the gas flow channels.[39,52] Most models have considered gas flow to be convective in the flow channels and diffusive from the flow channels to the catalyst layer in the GDL. Convective flow in the GDL has been considered in the case of interdigitated flow fields as a means to clear water from the pores of the GDL.[53–55]

The correlated motion of gas flow and water slugs between adjacent flow channels is a complex time dependent three-dimensional flow problem. There have been several steady state 3-D models of gas flows in PEM fuel cells, including a few that have considered the flow through the GDL under the rib.[41,42,51,56–58] But to the best of our knowledge, there have been no fuel cell models that considered gas flow being diverted between adjacent channels due to water slugs. Optimal flow channel designs will require 3-D time dependent PEM fuel cell models. These models should identify slug locations, local pressure, gas flow vectors, and regions of the flow field that are oxygen deficient. 3-D time dependent flow models accounting for slug formation and motion will be extremely computationally time intensive. We outline a simplified linear model describing the formation and motion of liquid slugs and gas in flow channels with a porous wall. The model attempts to address three essential questions: (1) When will slugs move? (2) When will they stall? (3) What force is necessary for slug motion?

To reduce the computation complexity, gas and liquid flows are decoupled. Slug growth and motion occur on a much longer time scale than altering the direction of gas flow. The coupled flow problem is broken up into a series of steady state gas flow problems where the constraints on the gas flow are periodically updated based formation or location of water slugs.

Figure 14 is a schematic of slug formation and motion based on the snapshot sequence shown in Figure 8. Gas flow is driven by through the flow channels or GDL by pressure differentials. The differential pressure for gas flow is assumed to be "zero" across a section of flow channel when no slugs occlude the channel. (Cheah et al. showed that growing drops pose little resistance to gas flow until the drops nearly span the cross-section of the channel and form slugs).[30] Slugs create resistances to flow; R_{channel} is the resistance for gas flow through the GDL beneath a slug in the channel and R_{rib} is the resistance for gas flow between adjacent channels beneath the rib. Each slug has a channel resistance given by Eq. 9, and each pair of slugs in adjacent channels has a rib resistance given by Eq. 10

$$R_{\text{channel}} = \frac{\mu_G L_{\text{slug}}}{k_{\substack{\text{GDL}\\\text{channel}}} wt_{\text{GDL}}} \tag{9}$$

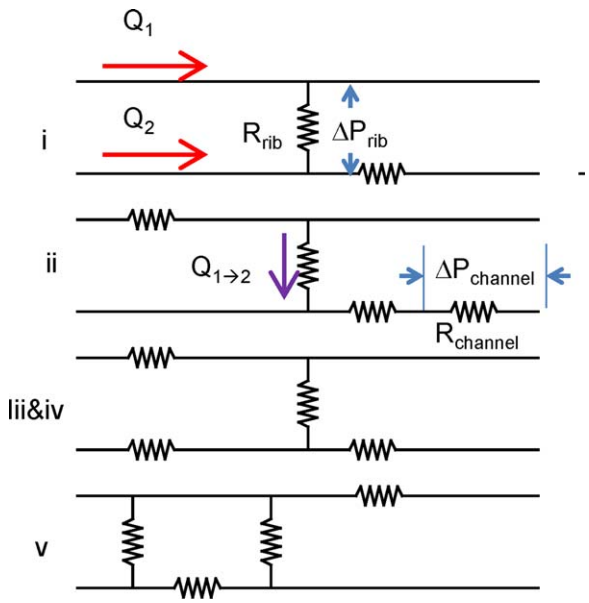

Figure 15. Electric circuit equivalent to the network transmission model for gas and liquid slug motion through parallel gas flow channels.

R_{channel} is the equivalent resistance for gas to flow the through the GDL underneath a slug of a gas flow channel. R_{rib} is the equivalent resistance for gas to flow through the GDL beneath the rib between adjacent channels. The different equivalent circuits correspond to the flow patterns shown in Figure 14. [Color figure can be viewed in the online issue, which is available at wileyonlinelibrary.com.]

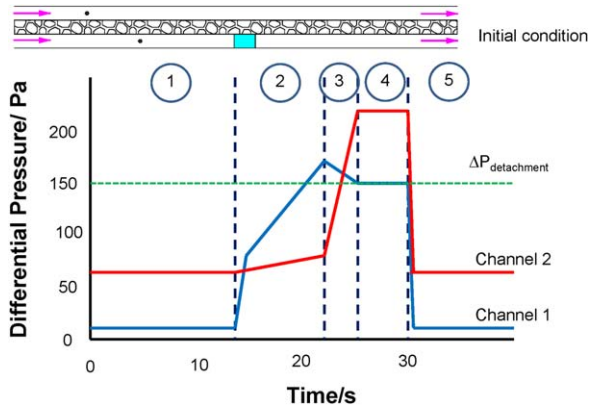

Figure 16. Predicted differential pressure profiles in Channels 1 and 2 for the flow in parallel gas flow channels.

The pressures are based on the Network transmission model. [Color figure can be viewed in the online issue, which is available at wileyonlinelibrary.com.]

$$R_{\text{rib}} = \frac{\mu_G w}{k_{\substack{\text{GDL}\\\text{rib}}}(\Delta L) t_{\text{GDL}}} \tag{10}$$

The distance ΔL in Eq. 10 is illustrated in Figure 14; it is the distance between slugs in adjacent channels, and it changes as slugs move in the channels. Both the channel resistance and the rib resistance change with time. R_{channel} increases as the slugs grow; R_{channel} reaches a maximum value when the slug detaches and begins to move. R_{rib} increases as slugs in adjacent channels approach each other. When R_{rib} increases the gas flow between adjacent channels is reduced which causes the detachment and motion of the slug in Channel 2.

The resistive elements for gas flow are shown in Figure 15. The gas network and flow resistances shown in Figure 14 are analogous to a simple electrical resistance network where gas flows are the equivalent currents and differential pressures are potential differences as illustrated in Figure 15. At any instant in time the differential pressures and gas flow rates along a channel or between adjacent channels can be solved for using Kirchhoff's law, with $\Delta P = Q_G R$ (the differential pressure equals the gas flow times the resistance to gas flow). A slug moves if $\Delta P_{\text{channel}} > \Delta P_{\text{detachment}}$. The slug moves at a velocity approximately given by Eq. 11

$$v_{\text{slug}} = \frac{1}{w^2}\left(Q_{\text{channel}} - \frac{\Delta P_{\text{detachment}}}{R_{\text{channel}}}\right) \tag{11}$$

$\Delta P_{\text{detachment}}$ is the differential pressure required for slug detachment and motion, and is given by Eq. 5. The differential pressure for slug motion is approximately independent of slug size.[26] The detachment pressure depends only on the interfacial force to advance the advancing and receding contact lines.[30]

The model assumes liquid water exists in one of four states in the flow channels.

State 1: Growing water drops attached to the inlet water pores from the GDL; these drops are stationary in position in the channel. The differential pressure across these growing drops is assumed to be zero. The volume increase of these drops as a function of time is equal to the liquid flow rates in the water pore.

State 2: Growing water slugs attached to the inlet water pores from the GDL. Slugs form when drops reach the critical length defined by Eq. 1. These slugs are stationary and remain stationary until the differential pressure (Eq. 3) is equal to the detachment pressure (Eq. 4). The volume increase of these slugs as a function of time is equal to the liquid feed rates to the water pores.

State 3: Moving water slugs. These are slugs that are moving in the channel. They do not change volume with time. The differential pressure for slug motion is given by Eq. 4. Slugs move with velocity v_{slug}, given by Eq. 11.

State 4: Stalled water slugs. These are slugs that have stopped moving in the channel. They do not change volume or position until the differential pressure across the slug increases above the detachment pressure.

This network model for multiphase flow assumes that the differential pressure for gas flow is the sum of three contributions (1) pressure to detach and move slugs, (2) pressure for gas flow to bypass a slug by flowing through the GDL underneath the slug, and (3) pressure for gas flow to bypass slugs by flow through the GDL beneath the rib into an adjacent channel. The model assumes that water exits from specific pores in the GDL and water does not re-enter the GDL after it forms drops or slugs in the gas flow channel. In our experiments with fuel cells, microfluidic flow experiments and surface wetting experiments we have never seen this condition violated with PTFE treated GDLs.

The assumptions of the transmission network model provide an algorithm to describe the gas flow and slug motion in a flow channel network:

1. The size and location of drops and slugs are enumerated.
2. The resistances for gas flow between drop and slug positions are enumerated and evaluated.

Table 4. Gas Flow and Slug Motion in Parallel Flow Channels

Time Period	Channel 1	Channel 2
1	Drop growth at water inlet pore	Drop growth at water inlet pore Stationary slug downstream
2	Slug growth at water inlet pore	Slug growth at water inlet pore Stationary slug downstream
3	Slug detachment and motion in Channel 1 Slug slows down as it approaches growing slug in Channel 2	Slug growth at water inlet pore Stationary slug downstream
4	Slug moves downstream in Channel 1	Slug detaches and begins to move in Channel 2 Stationary slug downstream
5	Slug exits from Channel 1	Moving slug slows down and stalls 1 mm short of touching the stationary slug in Channel 2

3. The state of each drop and slug are identified (i.e., drops and slugs are in one of the four states listed above).
4. Drops (State 1) have their sizes updated, increasing by $\Delta V = Q_L dt$.
5. Slugs attached to the inlet liquid pores (State 2) have their sizes updated, increasing by $\Delta V = Q_L dt$.
6. Moving slug (State 3) positions are updated by $\Delta x = v_{slug} dt$.
7. If a growing slug detaches a new drop is initiated at the inlet water pore.
8. Slugs that reach the end of a flow channel are removed from the system, when $x = L_{channel}$ the slug exits the system.
9. Stalled slugs (State 4) remain fixed in position and size.
10. Increment time and return to Step 1, $t_{i+1} = t_i + dt$.

Based on this algorithm the differential pressures in Channels 1 and 2 shown in Figure 14 may be predicted as a function of time based on a defined starting condition. Figure 16 shows the predicted differential pressure traces starting from Channel 1 empty and Channel 2 with a stalled slug 60 mm from the gas inlet. There are five time periods identified in Figure 16 which correspond to the time periods in Figure 8. The model has linearized all the pressure changes, but the agreement of the magnitudes of the pressure changes and the times for the transitions agree with the experimental results. The events occurring in each time period are summarized in Table 4.

Conclusions

Water slug formation and motion was studied in a microfluidic system that mimics the flow in adjacent gas flow channels of a PEM fuel cell. The system had two parallel flow channels separated by a rib. Water entered the channels from 100 μm pores through a GDL. Gas flow in adjacent channels communicates through the GDL beneath the rib separating the channels.

Water emerges from the GDL and grows into slugs that span the open area of the flow channel. Liquid slugs divert the gas flow through the GDL beneath the slug. The slugs detach and move when the pressure for gas flow through the GDL equals the pressure required to advance the gas/liquid/solid contact lines of the slug. The gas flow path depends on the permeability of the GDL, the slug volume and the presence of slugs in adjacent flow channels.

The permeability of a carbon paper GDL under the gas flow channel and beneath the rib between channels was measured by determining the detachment pressure for a slug, the slug length and the distance slugs travel as a function of gas flow rate. These measurements permitted the direct determination of GDL permeability under the channel and under the rib at different levels of compression of the GDL.

Slugs can be problematic in fuel cell operation as slugs hinder the supply of reactants from the gas flow channel through the GDL to the catalyst layer at the membrane/catalyst interface. The results presented in this article illustrate that liquid slugs divert gas flow through the GDL bypassing areas of the fuel cell.

The key results from this study are:

1. The porous GDL permits communication between adjacent flow channels. Gas flow can bypass slugs occluding the channel by flowing through the GDL.
2. Slugs detach and move when the pressure drop for gas to flow beneath the GDL under the slug is equal to the detachment pressure of the slug.
3. Slugs will stop moving when gas flow can bypass a slug and flow through the GDL under the rib into an adjacent gas flow channel.
4. Slugs in adjacent channels move synchronously when they are next to each other and gas flow between the flow channels is blocked.

Acknowledgments

Support from the following is acknowledged by the authors: national 863 high technology item (2012AA110601) and (2013AA110201). Donghao Ye thanks CSC for financial support. Eric Gauthier was supported by National Science Foundation Grant No. 0903661 "Nanotechnology for Clean Energy IGERT."

Literature Cited

1. Wang Y, Chen KS, Mishler J, Cho SC, Adroher XC. A review of polymer electrolyte membrane fuel cells: technology, applications, and needs on fundamental research. *Appl Energy*. 2011;88(4):981–1007.
2. Pratt JW, Klebanoff LE, Munoz-Ramos K, Akhil AA, Curgus DB, Schenkman BL. Proton exchange membrane fuel cells for electrical power generation on-board commercial airplanes. *Appl Energy*. 2013;101:776–796.
3. Owejan JP, Trabold TA, Jacobson DL, Arif M, Kandlikar SG. Effects of flow field and diffusion layer properties on water accumulation in a PEM fuel cell. *Int J Hydrogen Energy*. 2007;32(17):4489–4502.
4. Wilkinson DP, Vanderleeden O. Serpentine flow field design. In: Vielstich W, Lamm A, Gasteiger HA, editors. *Handbook of Fuel Cells, vol 3*. Hoboken, NJ: Wiley, 2003:315–324.
5. Corey TA. *Mechanics of Immiscible Fluids in Porous Media*. Highlands Ranch, CO: Water Resources Publications, 1994.
6. Heidary H, Kermani MJ. Performance enhancement of fuel cells using bipolar plate duct indentations. *Int J Hydrogen Energy*. 2013;38(13):5485–5496.
7. Hermann A, Chaudhuri T, Spagnol P. Bipolar plates for PEM fuel cells: a review. *Int J Hydrogen Energy*. 2005;30(12):1297–1302.
8. Antunes RA, de Oliveira MCL, Ett G, Ett V. Carbon materials in composite bipolar plates for polymer electrolyte membrane fuel cells: a review of the main challenges to improve electrical performance. *J Power Sources*. 2011;196(6):2945–2961.
9. Miyazawa A, Tada E, Nishikata A. Influence of corrosion of SS316L bipolar plate on PEFC performance. *J Power Sources*. 2013;231:226–233.
10. Oyarce A, Holmstrom N, Boden A, Lagergren C, Lindbergh G. Operating conditions affecting the contact resistance of bi-polar plates in proton exchange membrane fuel cells. *J Power Sources*. 2013;231:246–255.
11. Eom K, Cho E, Jang J, Kim HJ, Lim TH, Hong BK, Lee JH. Optimization of GDLs for high-performance PEMFC employing stainless steel bipolar plates. *Int J Hydrogen Energy*. 2013;38(14):6249–6260.
12. Grigoriev SA, Kalinnikov AA, Kuleshov NV, Millet P. Numerical optimization of bipolar plates and gas diffusion electrodes for PBI-based PEM fuel cells. *Int J Hydrogen Energy*. 2013;38(20):8557–8567.
13. Belchor PM, Forte MMC, Carpenter D. Parallel serpentine-baffle flow field design for water management in a proton exchange membrane fuel cell. *Int J Hydrogen Energy*. 2012;37(16):11904–11911.
14. Li H, Tang YH, Wang ZW, Shi Z, Wu SH, Song DT, Zhang JL, Fatih K, Zhang JJ, Wang HJ, Liu ZS, Abouatallah R, Mazza A. A review of water flooding issues in the proton exchange membrane fuel cell. *J Power Sources*. 2008;178(1):103–117.
15. Giurgea S, Tirnovan R, Hissel D, Outbib R. An analysis of fluidic voltage statistical correlation for a diagnosis of PEM fuel cell flooding. *Int J Hydrogen Energy*. 2013;38(11):4689–4696.
16. Misran E, Hassan NSM, Daud WRW, Majlan EH, Rosli MI. Water transport characteristics of a PEM fuel cell at various operating pressures and temperatures. *Int J Hydrogen Energy*. 2013;38(22):9401–9408.

17. Alink R, Haussmann J, Markotter H, Schwager M, Manke I, Gerteisen D. The influence of porous transport layer modifications on the water management in polymer electrolyte membrane fuel cells. *J Power Sources*. 2013;233:358–368.
18. Ye DH, Zhan ZG. A review on the sealing structures of membrane electrode assembly of proton exchange membrane fuel cells. *J Power Sources*. 2013;231:285–292.
19. Kitahara T, Nakajima H, Inamoto M, Morishita M. Novel hydrophilic and hydrophobic double microporous layer coated gas diffusion layer to enhance performance of polymer electrolyte fuel cells under both low and high humidity. *J Power Sources*. 2013;234:129–138.
20. Haussmann J, Markotter H, Alink R, Bauder A, Dittmann K, Manki I, Scholta J. Synchrotron radiography and tomography of water transport in perforated gas diffusion media. *J Power Sources*. 2013; 239:611–622.
21. Kimball EE, Benziger JB, Kevrekidis YG. Effects of GDL structure with an efficient approach to the management of liquid water in PEM fuel cells. *Fuel Cells*. 2010;10(4):530–544.
22. Park S, Lee JW, Popov BN. A review of gas diffusion layer in PEM fuel cells: materials and designs. *Int J Hydrogen Energy*. 2012; 37(7):5850–5865.
23. Kitahara T, Nakajima H, Inamoto M, Morishita M. Best combination of gas diffusion layers for polymer electrolyte fuel cell under cathode condition of very low humidity. *ECS Trans*. 2008;16(2):1603–1613.
24. Chun JH, Jo DH, Kim SG, Park SH, Lee CH, Kim SH. Improvement of the mechanical durability of micro porous layer in a proton exchange membrane fuel cell by elimination of surface cracks. *Renew Energy*. 2012;48:35–41.
25. Benziger J, Nehlsen J, Blackwell D, Brennan T, Itescu J. Water flow in the gas diffusion layer of PEM fuel cells. *J Membr Sci*. 2005;261: 98–106.
26. Colosqui CE, Cheah MJ, Kevrekidis IG, Benziger JB. Droplet and slug formation in polymer electrolyte membrane fuel cell flow channels: the role of interfacial forces. *J Power Sources*. 2011;196(23): 10057–10068.
27. Gauthier E, Duan Q, Hellstern T, Benziger J. Water flow in, through, and around the gas diffusion layer. *Fuel Cells*. 2012;12(5):835–847.
28. Kimball E, Whitaker T, Kevrekidis YG, Benziger JB. Drops, slugs, and flooding in polymer electrolyte membrane fuel cells. *AlChE J*. 2008;54(5):1313–1332.
29. Gauthier E, Hellstern T, Kevrekidis IG, Benziger J. Drop detachment and motion on fuel cell electrode materials. *ACS Appl Mater Interfaces*. 2012;4(2):761–771.
30. Cheah MJ, Kevrekidis IG, Benziger JB. Water slug formation and motion in gas flow channels: the effects of geometry, surface wettability, and gravity. *Langmuir*. 2013;29(31):9918–9934.
31. Ody CP. Capillary contributions to the dynamics of discrete slugs in microchannels. *Microfluid Nanofluidics*. 2010;9(2–3):397–410.
32. Trabold TA, Owejan JP, Jacobson DL, Arif M, Huffman PR. In situ investigation of water transport in an operating PEM fuel cell using neutron radiography: part 1—experimental method and serpentine flow field results. *Int J Heat Mass Transfer*. 2006;49(25–26):4712–4720.
33. Bazylak A, Heinrich J, Djilali N, Sinton D. Liquid water transport between graphite paper and a solid surface. *J Power Sources*. 2008; 185(2):1147–1153.
34. Theodorakakos A, Ous T, Gavaises A, Nouri JM, Nikolopoulos N, Yanagihara H. Dynamics of water droplets detached from porous surfaces of relevance to PEM fuel cells. *J Colloid Interface Sci*. 2006;300(2):673–687.
35. Cheah MJ, Kevrekidis IG, Benziger JB. Water slug to drop and film transitions in gas-flow channels. *Langmuir*. 2013;29(48):15122–15136.
36. Cho SC, Wang Y, Chen KS. Droplet dynamics in a polymer electrolyte fuel cell gas flow channel: forces, deformation and detachment. II: comparisons of analytical solution with numerical and experimental results. *J Power Sources*. 2012;210:191–197.
37. Hellstern T, Gauthier E, Cheah MJ, Benziger JB. The role of the gas diffusion layer on slug formation in gas flow channels of fuel cells. *Int J Hydrogen Energy*. 2013;38(35):15414–15427.
38. Bazylak A, Sinton D, Liu ZS, Djilali N. Effect of compression on liquid water transport and microstructure of PEMFC gas diffusion layers. *J Power Sources*. 2007;163(2):784–792.
39. Feser JP, Prasad AK, Advani SG. Experimental characterization of in-plane permeability of gas diffusion layers. *J Power Sources*. 2006;162(2):1226–1231.
40. Hussaini IS, Wang CY. Measurement of relative permeability of fuel cell diffusion media. *J Power Sources*. 2010;195(12):3830–3840.
41. Sun W, Peppley BA, Karan K. Modeling the influence of GDL and flow-field plate parameters on the reaction distribution in the PEMFC cathode catalyst layer. *J Power Sources*. 2005;144(1):42–53.
42. Zhou YB, Jiao K, Du Q, Yin Y, Li XG. Gas diffusion layer deformation and its effect on the transport characteristics and performance of proton exchange membrane fuel cell. *Int J Hydrogen Energy*. 2013;38(29):12891–12903.
43. Gaiselmann G, Totzke C, Manke I, Lehnert W, Schmidt V. 3D microstructure modeling of compressed fiber-based materials. *J Power Sources*. 2014;257:52–64.
44. Rama P, Liu Y, Chen R, Ostadi H, Jiang JK, Gao Y, Zhang X, Brivio D, Grassini P. A numerical study of structural change and anisotropic permeability in compressed carbon cloth polymer electrolyte fuel cell gas diffusion layers. *Fuel Cells*. 2011;11(2):274–285.
45. Totzke C, Gaiselmann G, Osenberg M, Bohner J, Arlt T, Markotter H, Hilger A, Wieder F, Kupsch A, Muller BR, Hentschel MP, Banhart J, Schmidt V, Lehnert W, Manke I. Three-dimensional study of compressed gas diffusion layers using synchrotron X-ray imaging. *J Power Sources*. 2014;253:123–131.
46. Zhang XM, Zhang XX. Impact of compression on effective thermal conductivity and diffusion coefficient of woven gas diffusion layers in polymer electrolyte fuel cells. *Fuel Cells*. 2014;14(2):303–311.
47. Burheim OS, Su HN, Hauge HH, Pasupathi S, Pollet BG. Study of thermal conductivity of PEM fuel cell catalyst layers. *Int J Hydrogen Energy*. 2014;39(17):9397–9408.
48. Ju H, Meng H, Wang CY. A single-phase, non-isothermal model for PEM fuel cells. *Int J Heat Mass Transfer*. 2005;48(7):1303–1315.
49. Ye DH, Gauthier E, Benziger JB, Pan M. Bulk and contact resistances of gas diffusion layers in proton exchange membrane fuel cells. *J Power Sources*. 2014;256:449–456.
50. Reshetenko TV, St-Pierre J, Rocheleau R. Effects of local gas diffusion layer gas permeability variations on spatial proton exchange membrane fuel cells performance. *J Power Sources*. 2013;241:597–607.
51. Bao N, Zhou YB, Jiao K, Yin Y, Du Q, Chen JX. Effect of gas diffusion layer deformation on liquid water transport in proton exchange membrane fuel cell. *Eng Appl Comput Fluid Mech*. 2014; 8(1):26–43.
52. Williams MV, Kunz HR, Fenton JM. Influence of convection through gas-diffusion layers on limiting current in PEM FCs using a serpentine flow field. *J Electrochem Soc*. 2004;151(10):A1617–A1627.
53. Van Nguyen T, Knobbe MW. A liquid water management strategy for PEM fuel cell stacks. *J Power Sources*. 2003;114(1):70–79.
54. Hu MR, Gu AZ, Wang MH, Zhu XJ, Yu LJ. Three dimensional, two phase flow mathematical model for PEM fuel cell: part I. *Model development*. *Energy Convers Manag*. 2004;45(11–12):1861–1882.
55. Birgersson E, Vynnycky M. A quantitative study of the effect of flow-distributor geometry in the cathode of a PEM fuel cell. *J Power Sources*. 2006;153(1):76–88.
56. Suga K, Nishimura W, Yamamoto T, Kaneda M. Measurements of serpentine channel flow characteristics for a proton exchange membrane fuel cell. *Int J Hydrogen Energy*. 2014;39(11):5942–5954.
57. Berning T, Djilali N. A 3D, multiphase, multicomponent model of the cathode and anode of a PEM fuel cell. *J Electrochem Soc*. 2003; 150(12):A1589–A1598.
58. Park J, Li XG. An analytical analysis on the cross flow in a PEM fuel cell with serpentine flow channel. *Int J Energy Res*. 2011;35(7): 583–593.

Manuscript received Aug. 21, 2014, and revision received Oct. 6, 2014.